

Article

Facile Preparation and Characterization of Silica Nanoparticles from South Africa Fly Ash Using a Sol–Gel Hydrothermal Method

Patrick Ehi Imoisili, Emeka Charles Nwanna  and Tien-Chien Jen * 

Mechanical Engineering Science Department, Faculty of Engineering and the Built Environment, University of Johannesburg, Kingsway and University Road, Auckland Park, P.O. Box 524, Johannesburg 2006, South Africa

* Correspondence: tjen@uj.ac.za

Abstract: Silica nanoparticles (SNPs) consist of several applications which include lightweight aggregates, energy storage, and drug delivery. Nevertheless, the silica reagents used in SNP synthesis are both costly and hazardous. As a result, it is critical to look for other sources of silica. For this research, a simple sol–gel hydrothermal approach is used to make SNPs from South African fly ash (SAFA). SAFA is classified as fly ash class F according to X-ray fluorescence (XRF) analysis. The wide-angle X-ray diffraction (XRD) pattern reveals the structural composition of SAFA and the amorphous phase of extracted SNPs, while Fourier transform infrared (FTIR) examination reveals the presence of silanol and siloxane groups. Basic SNPs were generally spherical with diameters of about 60 nm, according to scanning electron microscopy (SEM) and transition electron microscope (TEM) studies. The presence of SiO₂ is confirmed by energy-dispersive X-ray spectroscopy (EDX) spectrum analysis. Particle size assessment indicates particle sizes ranging from 48 nm to 87 nm in diameter, with a mean diameter of 67 nm. The application of SNPs in wastewater treatment demonstrated that they can be used to remove Cd²⁺ from an aqueous solution. This research offers new ideas for using South African fly ash in SNP manufacturing.



Citation: Imoisili, P.E.; Nwanna, E.C.; Jen, T.-C. Facile Preparation and Characterization of Silica Nanoparticles from South Africa Fly Ash Using a Sol–Gel Hydrothermal Method. *Processes* **2022**, *10*, 2440. <https://doi.org/10.3390/pr10112440>

Academic Editor: Fabio Carniato

Received: 23 October 2022

Accepted: 15 November 2022

Published: 18 November 2022

Publisher's Note: MDPI stays neutral with regard to jurisdictional claims in published maps and institutional affiliations.



Copyright: © 2022 by the authors. Licensee MDPI, Basel, Switzerland. This article is an open access article distributed under the terms and conditions of the Creative Commons Attribution (CC BY) license (<https://creativecommons.org/licenses/by/4.0/>).

Keywords: silica; nanoparticles; fly ash; sol–gel; hydrothermal

1. Introduction

A byproduct of burning coal in a thermal power station is fly ash. Eskom, South Africa's national power company, generates 34 million tonnes of coal fly ash annually from the use of about 120 million tonnes of coal, of which 95% is not recycled and the remaining 5% is recycled in the cement and building materials industries [1]. Fly ash is made up of mostly spherical, solid/hollow, and amorphous pieces of tiny, powdery particles [2], and it has a low bulk density and a great amount of distinct surface area [3]. Fly ash can range in hue from a deep red to orange, blue, white, or even yellow depending on the amount of unburned carbon and iron present. Coal ash has a specific gravity that is usually about 2.0, but to a great extent, ranges from 1.6 to 3.1.

A combination of several factors, inclusive of the shape of the particle, gradation, as well as chemical composition, are accountable for this variation [4]. Based on its Si, Al, and Fe oxide material, fly ash has been classified into two groups per ASTM C618 [5]. Fly ash is rated as class C or F. Fly Ash grade C is found to consist of high calcium content, while grade F, is rich in silica material [5]. However, it is getting more difficult to identify the character of fly ash because of its heterogeneous structure and physical characteristics. Catalysts alongside catalyst aids, pigments, adsorbents, mechanical substrates, electrical and thermal insulators, thin film substrates, and exhaust gas filters are examples of silica applications [6–11].

As a result of its large aluminum (Al) and silicon (Si) composition, fly ash could be a useful supplementary resource of refined alumina and silica, assuming that sufficient commercially viable processes can be established [12]. With the use of chemical vapor condensation (CVC) [13], reverse microemulsion (RME) [14], precipitation [15], and the sol–gel method [16–18], silica has successfully been isolated from a range of agricultural bio-resources, including sugarcane [19–22], rice husk ash [23–27], maize cob ash [28–32], bagasse ash [33], clay [34], wheat husk ash, and coffee husk ash, [35–37]. Owing to its large concentration of SiO_2 and Al_2O_3 , various research has explored coal fly ash from the synthesis of silica. Silica from coal ash can also be employed for adsorption or the retention of certain heavy metals from wastewater [38–41], either explicitly or as fillers in a polymer matrix. It was discovered that the mineralogical and chemical makeup of the generated material was just as vital as the Si quantity in fly ash together with its retrieval [41,42].

When tolerable amounts of cadmium, Cd (II), and other metals are surpassed in the aquatic environment, they have the potential to harm human physiology along with other biological systems [43]. Heavy metals cannot be ruined or deteriorated in any way. The toxicity of heavy metals could result from polluted drinking water (e.g., lead pipes), elevated concentrations of the surrounding air close to emission sources, or consumption via the food chain [44]. Due to the obvious rising usage of heavy metals in industry, metallic compounds are more readily available in natural water sources [45,46]. Metal contaminants have been removed from water using a variety of processes, including adsorption, precipitation, membrane filtration, and ion exchange [47]. Adsorption, on the other hand, is a cost-effective and efficient method of eliminating heavy metals, organic contaminants, and dyes from contaminated waterways.

The preparation of silica nanoparticles from South African fly ash has been restricted and limited to a solitary study by Mathibela et al. (2020). They synthesized SNPs from a sol–gel process with the utilization of sulphuric acid as the catalyst, polyethylene glycol (PEG) as the surfactant, and reported 99.3 wt. %, SiO_2 purity, and 26% yield [12]. From previous research, 37.3% [38] and about 62% SiO_2 [39] have been reported from Chinese fly ash. According to the author's expertise, there has been no exposition of the sol–gel hydrothermal template-free synthesis method for silica preparation from SAFA. In this study, a facile extraction of silica from South African fly ash (SAFA) was carried out using a sol–gel, hydrothermal template-free method. Extracted silica was characterized by X-ray diffraction (XRD), X-ray fluorescence (XRF), scanning electron microscope (SEM)/energy-dispersive X-ray spectroscopy (EDX), Fourier transform infrared spectroscopy (FTIR), and transition electron microscope (TEM). In addition, prepared SNPs were exploited for the elimination of Cd (II), from wastewater.

2. Experiment

2.1. Material and Methods

Coal fly ash was gathered from Lethabo power station in South Africa. Unburned carbon and floating beads were removed from the samples using froth flotation [48].

2.2. Silica Extraction

The extraction process of silica from South African fly ash (SAFA) was carried out via a sol–gel, hydrothermal template-free method. SAFA samples containing 50 g (Figure 1a) were introduced to 500 mL of 2 M NaOH in a beaker and heated at 100 °C on a hotplate for 2 h. The solution was stirred incessantly to liquefy the presence of silica in the SAFA, thereby obtaining a solution of sodium silicate. This solution then underwent filtration with the use of filter paper, with deionized water used in washing the residue. The filtrate was allowed to cool and thereafter, underwent titration with a 2 M HCl up to a pH range of 7.5–8.0. The sample solution was poured into a Teflon autoclave and later put into a muffle furnace for 24 h at 373 K for the hydrothermal process to yield silica aqua gels (Figure 1b). The silica aqua gels were refluxed with 1 M HCl for 2 h and dissolved in 1 M NaOH with constant stirring for 1 h. After, the solution was titrated with 1 M HCl to

pH 7.5. The resulting white silica xerogel (Figure 1c) was dried at 80 °C and subjected to successive washing cycles. This way, minerals, and impurities are easily separated from the silica. This is because it is more effective to wash dried silica (xerogel) in distilled water (dH₂O) than to wash silica gel (aquagel) before drying, to extract the silica minerals [31]. The extracted SNPs were dried at 110 °C for 6 h (Figure 1d). To measure the production of SNPs concerning the SAFA composition and the purity level of the final SNPs, the product masses were reported by the XRF analysis in Table 1.

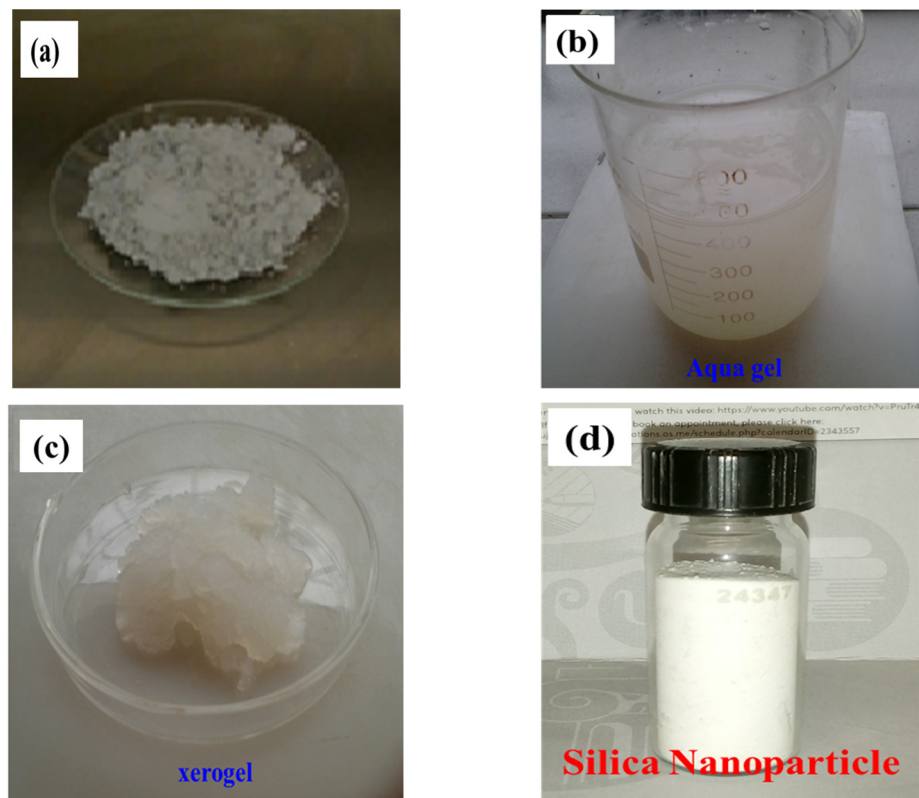


Figure 1. (a) SAFA, (b) silica aquagel, (c) silica xerogel, (d) silica nanoparticles.

Table 1. XRF analysis of SAFA and SNP.

Composition	Concentration Wt. (%)	
	SAFA	SNP
Al ₂ O ₃	31.66	0.15
BaO	0.19	0.00
CaO	5.33	0.02
Cr ₂ O ₃	0.06	0.00
Fe ₂ O ₃	4.10	0.05
K ₂ O	0.84	0.03
MgO	1.54	0.00
Na ₂ O	0.20	0.01
P ₂ O ₅	0.66	0.00
SiO ₂	52.03	98.76
SO ₃	0.35	0.00
TiO ₂	1.72	0.00
LOI	1.33	0.98
Total	100.00	100.00

2.3. Characterizations

Elemental composition was determined by the “MagiX PRO” wavelength dispersive XRF spectrometer from PANalytical. XRD analysis of crystal structure was analyzed using Philips/PANalytical X’Pert Powder Diffractometer at 40 kV acceleration voltage as well as a 40 mA current from 2θ 15° to 55°. Surface morphology was analyzed using a TESCAN VEGA3 SEM. TEM was performed using a JEM-2100 JEOL electron microscope attached with Oxford X-Max for EDX analysis. The surface area of the samples was studied by Brunauer-Emmett-Teller (BET), using a micrometric ASAP 2460. Inductively Coupled Plasma Optical Emission spectroscopy systems (ICP-OES) analysis was utilized for sorption analysis, and IRAffinity-IS was utilized for FTIR analysis. Hitachi STA TG/DSC was used for TGA/DTA analysis, while UV-1800 spectrophotometer was used for ultraviolet-visible diffuse reflection spectroscopy (UV-vis DRS) analysis.

2.4. Application of Extracted SNPs in the Removal of Cd^{2+} from Aqueous Solution

The influence of the quantity of sorbent (m/V, 0.50 g/L, 0.74 g/L, and 1.00 g/L) and removal efficiency on the initial concentration of Cd^{2+} in an aqueous solution was investigated. Cd^{2+} solutions were made by deliquescing various quantities of cadmium nitrate in a 1 L dH₂O. Across all the sorption studies, 50 mL of Cd^{2+} solution was used, and the solution’s pH was changed by 0.1 M NaOH or 1 M HCl. For Inductively Coupled Plasma Optical Emission spectroscopy systems (ICP-OES) analysis, the solution underwent filtration via a filter membrane of 0.45 μm after sorption. The precise Cd^{2+} concentration in the initial solution alongside the filtrate after the sorption process was measured. The operating solution’s pH was modified to pH 5.0 using 1.0 M HCl or 0.1 M NaOH based on a previous study [38,40]. Each sorption was performed in triplicate at 30 °C, and 240 min of reaction time. The sorption capacity (q_e) and the efficiency of removal were estimated from Equations (1) and (2).

$$q_e = \frac{(C_o - C_e)V}{m} \quad (1)$$

$$\text{Removal efficiency (\%)} = \frac{(C_o - C_e)}{C_o} \quad (2)$$

where C_o and C_e are metal concentrations at initial and final concentrations, respectively; sorbent mass = m , and solution volume is V .

3. Results and Discussions

3.1. XRF Analysis

The constituent composition of SAFA as determined by XRF analysis is shown in Table 1. It contains mainly Al_2O_3 (31.66%), SiO_2 (52.03%), Fe_2O_3 (4.10%), and CaO (5.33%). After extraction, SNP yield from SAFA was 28.6%, and silica content was 98.56%; this was slightly higher than 24% and similar to 99.3% previously reported using the template method [7]. According to the American Society for Testing and Materials (ASTM C618), this SAFA can be classified as class F owing to its large composition of alumina and silica [5].

3.2. XRD Analysis

Analysis from the XRD of SAFA and SNP illustrated in Figure 2 reveals that SAFA samples contain crystalline phases of Hydrosodalite [$\text{Na}_8(\text{AlSiO}_4)_6(\text{OH})_2 \cdot n\text{H}_2\text{O}$], Anhydrite [CaSO_4], Quartz (SiO_2), and Mullite ($\text{Al}_6\text{Si}_2\text{O}_{13}$), with a substantial silica amorphous phase at 2-theta 19–25°. This had similarities with prior reports from disparate coal fly ash [4,49]. A broad diffraction peak was observed for SNP at 2-theta = 19–25°. It was however observed that the broad peak correlated to the amorphous fraction has been shifted to lower 2-theta angles in sample SNP compared to sample SAFA. The broad diffraction peak confirms the predominantly amorphous nature of extracted SNPs [12,16,31]. This was consistent with the ICDD database PDF # 01-089-8935.

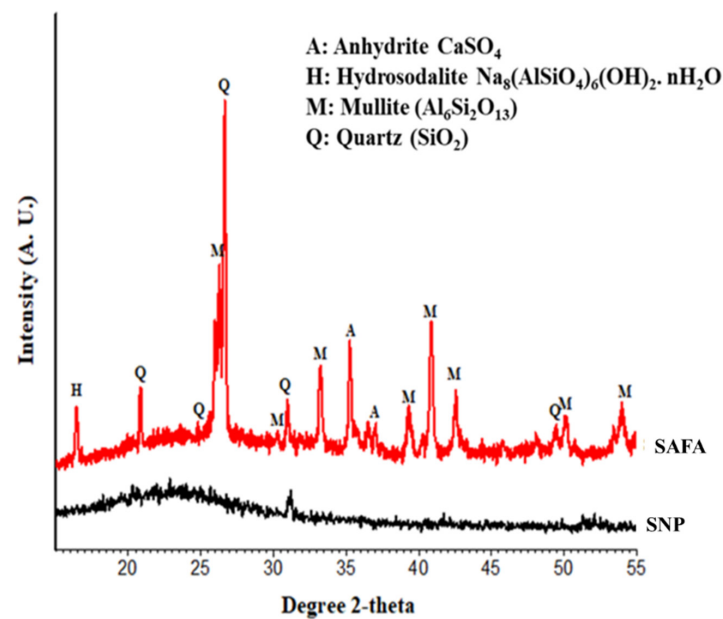


Figure 2. XRD analysis of SAFA and SNP.

3.3. FTIR Analysis

FTIR spectra are shown in Figure 3. The O-Si-O vibrational modes characteristic peak was noticed at 472 cm^{-1} [50]. The Si-O stretching vibration was detected at 581 cm^{-1} , symmetrical stretching vibration network of Si-O-Si was assigned to 807 cm^{-1} [17,18]. Band 1071 cm^{-1} was because of the intermittent stretch vibration due to Si-O-Si that is typical of SNPs [12,31], this band was observed to have higher intensity in the extracted SNPs. The O-H bond symmetric bending was observed at the 1419 cm^{-1} band [23], and the 1652 cm^{-1} broadband was a result of the O-H bond bending vibration which emanated from the Si-OH silanol group. While the 3452 cm^{-1} and 3471.13 cm^{-1} bands were because of the O-H bond stretching vibration of the Si-OH silanol group which is a result of the silica surface adsorbed H_2O molecules [23,32,51]. SAFA includes more adsorbed water molecules than SNPs, implying that the samples are mostly made up of adsorbed water. However, after silica extraction, the amount of adsorbed water decreases.

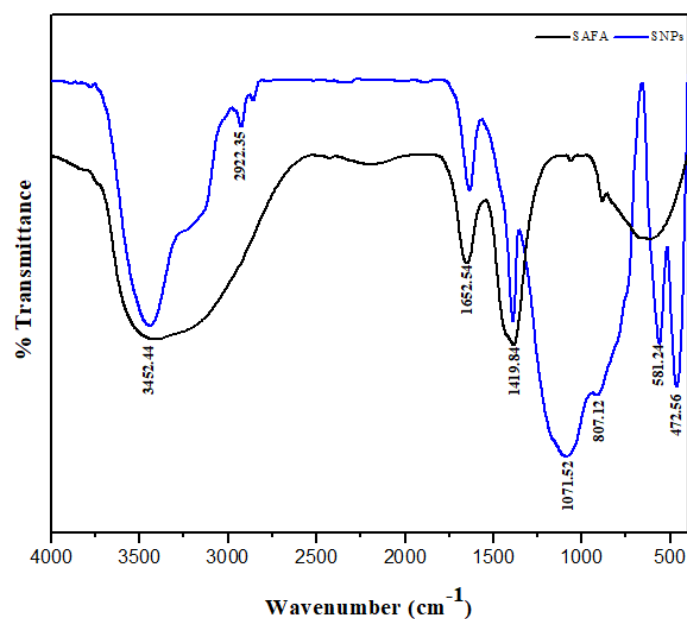


Figure 3. FTIR spectral of SAFA and extracted SNPs.

3.4. SEM/TEM Analysis

The morphology of SAFA particles is shown in Figure 4a. From the SEM image, SAFA occurs as a set of particles with unusual shapes, as well as spheroidal and ellipsoidal bodies of different measurements. These discoveries are in good alignment with those stated by Kutchko et al. [2] and Zhu et al. [52], respectively. These earlier experiments have shown that SAFA particle diameter is inconsistent, with small-sized particles adhering to the surfaces of certain spheroidal bodies, which were as well discovered within this research. SEM image of SNP, as shown in Figure 4b, revealed that primary SNPs formed agglomeration. SEM investigation through the Scanning Probe Image Processor revealed particle size variation between 64 nm and 97 nm diameter, with a 65 nm mean size diameter.

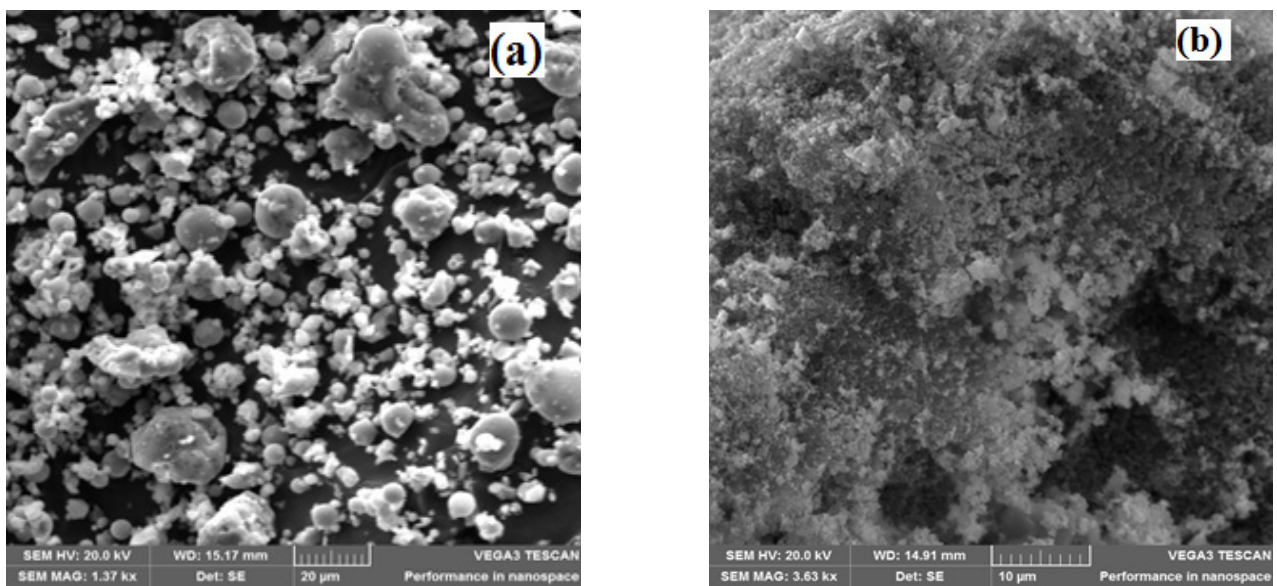


Figure 4. (a) SEM image of SAFA, (b) SEM image of SNPs.

TEM of SNPs depicted in Figure 5a, revealed that primary SNPs were roughly spherical with sizes of about ≥ 60 nm and aggregated to form an agglomeration of micron-size. Strong Si, and O intensity illustrated in the EDX Spectrum of Figure 5b, certified silica (SiO_2) to be the sample's prevailing element. This is around 98% of the overall component. The presence of C and Cu is from the carbon-coated copper grids used in the TEM analysis. There are however negligible impurities that are usually associated with the process of sol-gel extraction. Strong peak intensities of Si and O demonstrated in Figure 4 (EDX Spectrum), indicated silica (SiO_2) as the principal material of the sample. This represents approximately 98.56% of the total material.

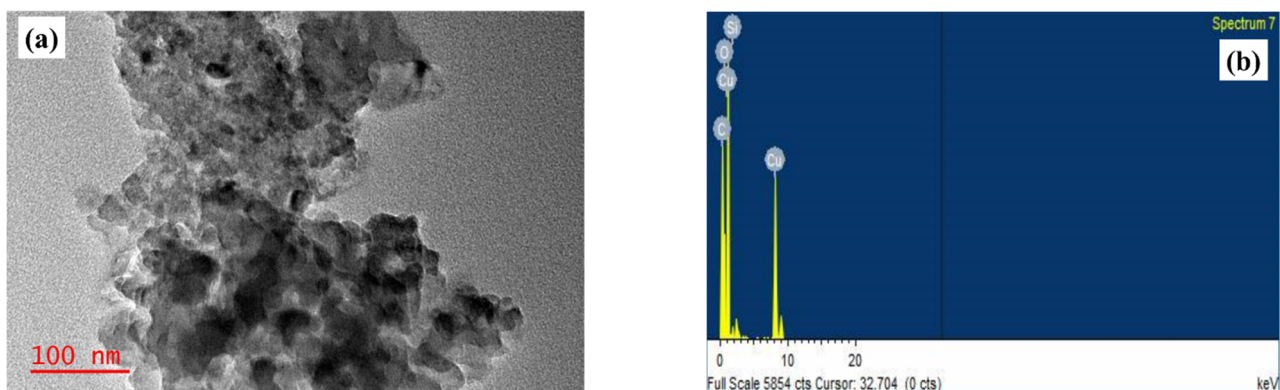


Figure 5. (a) TEM image of SNP (b) EDX of SNP.

3.5. Bandgap

The prepared SNP optical bandgap (E_g) was evaluated through the measurement of powdered spectral absorption via UV–vis absorbance spectroscopy. The bandgap was subsequently extracted from the resulting tauc plot (Figure 6). The (hv) quantity is displayed along the abscissa in a standard tauc plot while being depicted along the ordinate. The relationship between the photon energy (h) and absorption coefficient (α) demonstrated in Equation (3), can be applied in the calculation of the bandgap.

$$(\alpha hv)^2 = c (hv - E_g) \quad (3)$$

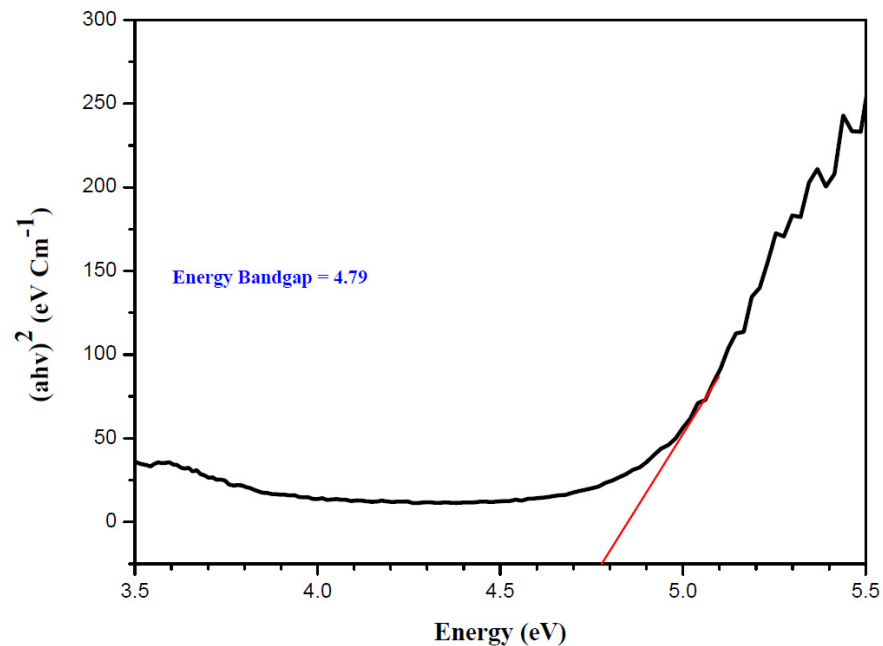


Figure 6. The energy band gap of extracted SNPs.

From the equation, α symbolizes the optical coefficient of absorption, c designates the direct transition constant, with h represented as Planck's constant, and ν denoting the incident photon frequency. The linear intercept of the curve of $(\alpha hv)^2$ vs energy ($h\nu$), was used to evaluate the optical bandgap of the material [53]. The band gap of the prepared SNPs was reported as 4.79 eV. This was lower than the previously reported value by Maj, S. (1988) [54] and similar to the 4.25 eV reported by Khedkar et al. (2019) [55].

3.5.1. Thermal Analysis (TGA-DTA)

From the TGA-DTA illustrated in Figure 7, a weight loss of two-step could be recognized. This weight loss which measured 143 °C (step 1) was attributed to the physically adsorbed dehydration of H₂O. The chemical-bound water from the preparation technique was allotted to the minimal weight loss observed within 143 °C and 535 °C (step 2) [16]. Beyond 535 °C, there was no more weight loss observed, indicating that the retrieved SNPs had reached thermal stabilization. Sharp endothermic peaks within the DTA investigation of a comparable temperature range supported this conclusion [56]. However, beyond 765 °C (stage 3), there was a shape weight loss seen, and the amorphous silica transforms into crystalline silica.

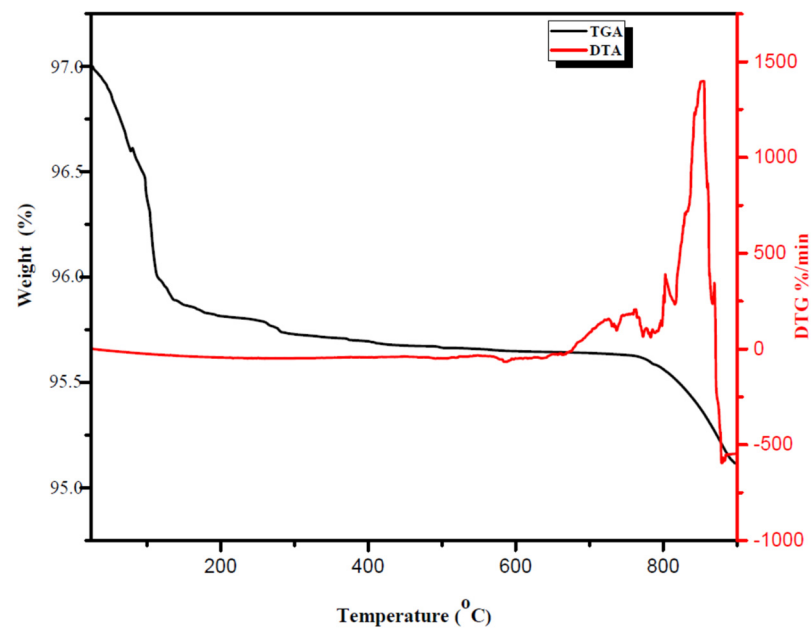


Figure 7. TGA-DTA curves of SNPs.

3.5.2. BET Surface Area (S_{BET}) Analysis

Nitrogen adsorption/desorption isotherms of extracted SNPs prepared from SAFA are displayed in Figure 8. Following the classification system used by the International Union of Pure and Applied Chemistry (IUPAC), the isotherm appeared to be that of TYPE IV with a well-defined peak at high P/P_0 , which is typical of mesoporous materials [16,57,58]. A large surface area of $18,651 \text{ m}^2/\text{g}$ was also reported in this study. The surface area of prepared nano silica and their sources are shown in Table 2.

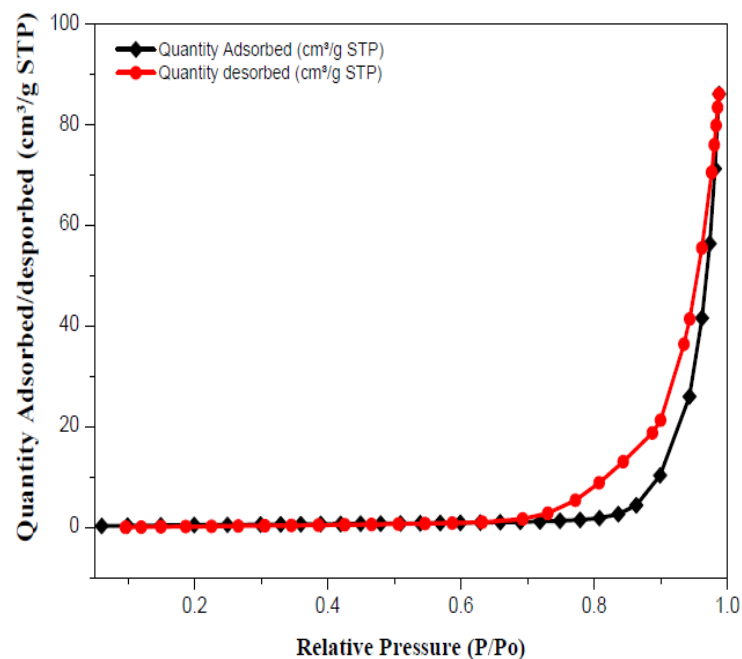
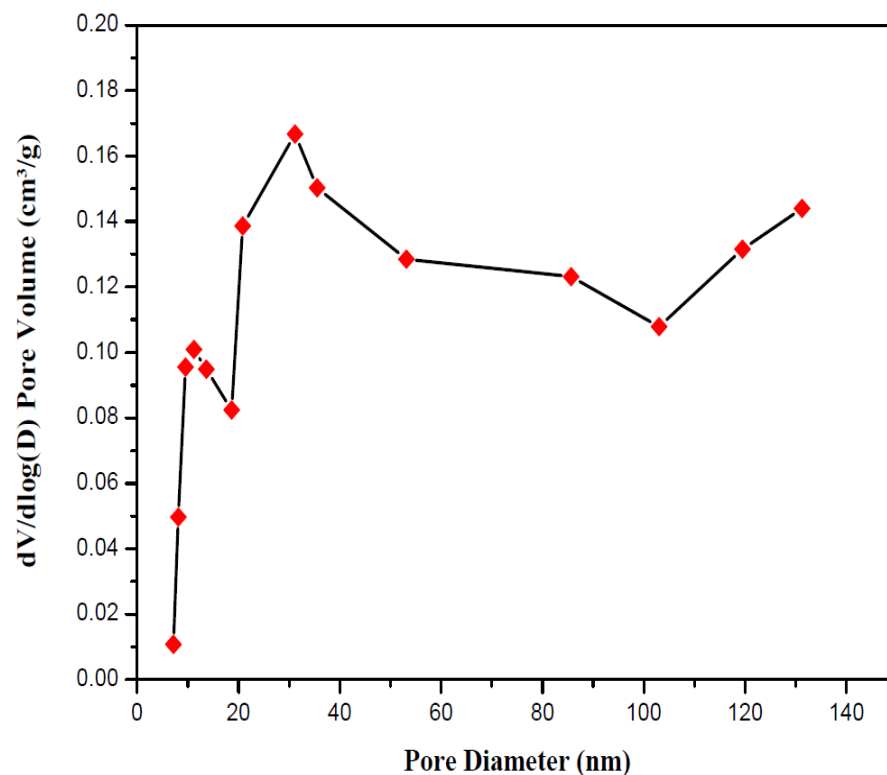


Figure 8. Adsorption-desorption SNPs isotherms of N_2 .

Table 2. Surface area of previously prepared nano silica.

Sources	Surface Area ($\text{m}^2 \text{g}^{-1}$)	References
Palm kernel shell ash	438	[59]
Rice Husk	327	[60]
Silica-rich rock	422	[61]
Coal Fly Ash	1865	[62]
Oil Shale ash	697	[63]

The prepared SNPs' pore size distribution was determined using desorption isotherms by the Barrett–Joyner–Halenda (BJH) approach as shown in Figure 9. At high corresponding pressures of 0.7 and 1.0, respectively, the isotherms exhibited a unique hysteresis loop type H3, which displayed the existence of 35.71% mesoporous SNPs (2–50 nm) and 64.29% microporous SNPs (above 50 nm), exhibiting a bimodal distribution. The average pore diameter was determined as 46.3 nm.

**Figure 9.** Pore size distribution of SNPs.

3.5.3. Cd^{2+} Removal from Aqueous Solution Utilizing Prepared SNPs

The sorption behavior may be influenced by the original concentrations of metal ions and the dosage of SNPs. The original Cd^{2+} concentration affected SNPs sorption positively. Figure 10 explained that the reduced dosages of 0.5 g/L and 0.75 g/L resulted in the system achieving faster sorption saturation with an increasing original Cd^{2+} concentration. This thus suggests reduced sorption capacities. Similar results have been previously reported [38,40]. As shown in Figure 11, the purge efficacy of Cd^{2+} swiftly decreases with increasing initial concentrations of 0.05 g/L and 0.75 g/L dosages accordingly. However, a 1.00 g/L dosage suggests a higher sorption capacity of SNPs at a higher dosage.

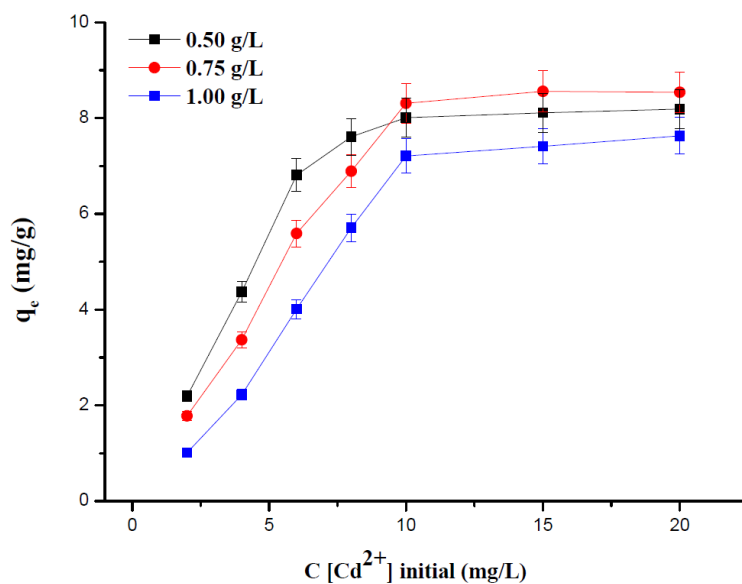


Figure 10. The initial concentrations of Cd²⁺ as a function of SNPs dosage (T = 30 °C, pH = 5).

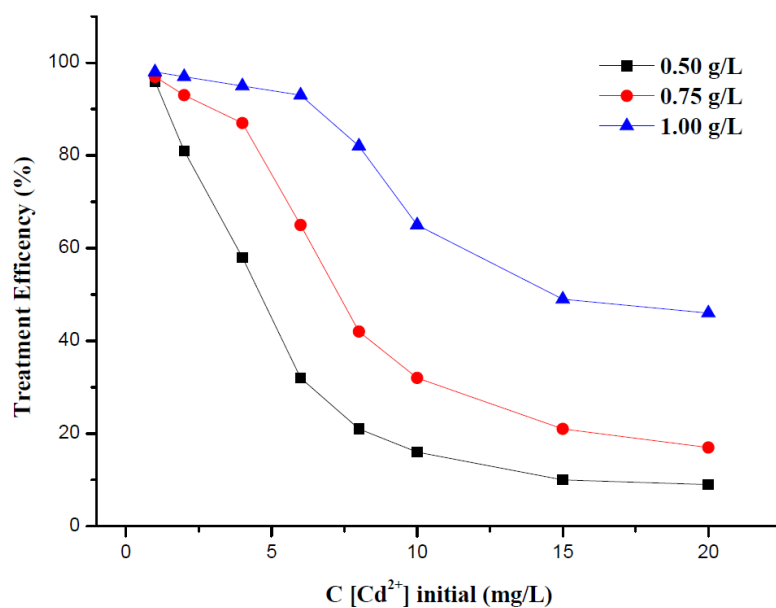


Figure 11. Original concentrations of Cd²⁺ as a function of SNPs removal efficiency (T = 30 °C, pH = 5).

4. Conclusions

SNPs were extracted using a sol–gel hydrothermal template-free technique from South Africa Fly Ash (SAFA). The occurrence of silica in SAFA and the amorphous nature of derived silica have been discovered by XRF studies. Extracted silica yield was 28.6% and purity was 98.56% with a negligible mineral contaminant. The crystalline phase of SAFA and the amorphous nature of extracted SNP have been investigated by XRD. The existence of SiO₂ in the samples was confirmed by EDX results, with the FTIR data displaying the primary chemical group present in the samples. SEM and TEM revealed that primary SNPs were roughly spherical with sizes of about ≥ 60 nm. This study will add to the awareness of a template-free, low-cost extraction of SNPs from SAFA, as well as being a great performance and economical sorbent for disposing of wastewater by the materials which emanate from waste. The efficient use of SAFA can have significant economic and environmental benefits as a useful raw material for advanced high-tech applications.

Author Contributions: Conceptualization, writing of the original draft of the article, reviewing, Validation. P.E.I.; methodology, and editing of the original draft. E.C.N.; Resources, Reviewing & Editing, Supervision. T.-C.J. All authors have read and agreed to the published version of the manuscript.

Funding: The authors acknowledge the Global Excellence Stature (GES), the National Research Foundation (NRF) of South Africa, as well as the University Research Council (URC) for financial support.

Data Availability Statement: Data availability on request.

Conflicts of Interest: The authors declare no conflict of interest.

References

1. British Petroleum. BP Energy Outlook: 2018 Edition. 2018. Available online: <https://www.bp.com/content/dam/bp/en/corporate/pdf/energy-economics/energy-outlook/bp-energy-outlook-2018.pdf> (accessed on 12 August 2018).
2. Kutchko, B.G.; Kim, A.G. Fly ash characterization by SEM-EDS. *Fuel* **2006**, *85*, 2537–2544. [[CrossRef](#)]
3. Ismail, K.N.; Hussin, K.; Idris, M.S. Physical, chemical & mineralogical properties of fly ash. *J. Nucl. Relat. Technol.* **2007**, *4*, 47–51.
4. Liu, C.L.; Zheng, S.L.; Ma, S.H.; Luo, Y.; Ding, J.; Wang, X.H.; Zhang, Y. A novel process to enrich alumina and prepare silica nanoparticles from high-alumina fly ash. *Fuel Process. Technol.* **2018**, *173*, 40–47. [[CrossRef](#)]
5. American Society for Testing and Materials. *ASTM C618, Annual Book of ASTM Standard*; ASTM International: West Conshohocken, PA, USA, 2004.
6. Naik, S.P.; Sokolov, I. Room temperature synthesis of nanoporous silica spheres and their formation mechanism. *Solid State Commun.* **2007**, *144*, 437–440. [[CrossRef](#)]
7. Venkateswara Rao, A.; Hegde, N.D.; Hirashima, H. Absorption and desorption of organic liquids in elastic superhydrophobic silica aerogels. *J. Colloid Interface Sci.* **2007**, *305*, 124–132. [[CrossRef](#)]
8. Yang, M.; Wang, G.; Yang, Z. Synthesis of hollow spheres with mesoporous silica nanoparticles shell. *Mater. Chem. Phys.* **2008**, *111*, 5–8. [[CrossRef](#)]
9. Zaky, R.R.; Hessien, M.M.; El-Midany, A.A.; Khedr, M.H.; Abdel-Aal, E.A.; El-Barawy, K.A. Preparation of silica nanoparticles from semi-burned rice straw ash. *Powder Technol.* **2008**, *185*, 31–35. [[CrossRef](#)]
10. Jesionowski, T. Synthesis and characterization of spherical silica precipitated via emulsion route. *J. Mater. Process. Technol.* **2008**, *203*, 121–128. [[CrossRef](#)]
11. Bernardos, A.; Kourimská, L. Applications of mesoporous silica materials in food—A review. *Czech J. Food Sci.* **2013**, *31*, 99–107. [[CrossRef](#)]
12. Aphane, M.E.; Doucet, F.J.; Kruger, R.A.; Petrik, L.; van der Merwe, E.M. Preparation of Sodium Silicate Solutions and Silica Nanoparticles from South African Coal Fly Ash. *Waste Biomass Valor.* **2020**, *11*, 4403–4417. [[CrossRef](#)]
13. Bagwe, R.P.; Hilliard, L.R.; Tan, W. Surface modification of silica nanoparticles to reduce aggregation and nonspecific binding. *Langmuir* **2006**, *22*, 4357–4362. [[CrossRef](#)]
14. Liu, S.; Han, M.-Y. Silica-coated metal nanoparticles. *Chemistry* **2010**, *5*, 36. [[CrossRef](#)]
15. Jal, P.K.; Sudarshan, M.; Saha, A.; Sabita, P.; Mishra, B.K. Synthesis and characterization of nano-silica prepared by precipitation method. *Colloid. Surf.* **2004**, *240*, 173–178. [[CrossRef](#)]
16. Imoisili, P.E.; Jen, T.C.; Safaei, B. Microwave-assisted sol-gel synthesis of TiO₂-mixed metal oxide nanocatalyst for degradation of organic pollutant. *Nanotechnol. Rev.* **2021**, *10*, 1–11. [[CrossRef](#)]
17. Imoisili, P.E.; Ukoba, K.O.; Jen, T.C. Synthesis and characterization of amorphous mesoporous silica from palm kernel shell ash. *Bol. Soc. Esp. Cerám. Vidr.* **2020**, *59*, 159–164. [[CrossRef](#)]
18. Ntobeng, M.K.; Imoisili, P.E.; Jen, T.C. Synthesis and photocatalytic performance of Ag-TiVOX nanocomposite. *J. King Saud Uni-Sci.* **2020**, *32*, 3103–3110. [[CrossRef](#)]
19. Channoy, C.; Maneewan, S.; Punlek, C.; Chirarattananon, S. Preparation and characterization of silica gel from bagasseash. *Adv. Mater. Res.* **2018**, *1145*, 44–48.
20. Rovani, S.; Santos, J.J.; Corio, P.; Fungaro, D.A. Highly pure silica nanoparticles with high adsorption capacity obtained from sugarcane waste ash. *ACS Omega* **2018**, *3*, 2618–2627. [[CrossRef](#)]
21. Sapawe, N.; Osman, N.S.; Zakaria, M.Z.; Fikry, S.A.S.S.M.; Aris, M.A.M. Synthesis of green silica from agricultural waste by sol-gel method. *Mater. Today Proc.* **2018**, *5*, 21861–21866. [[CrossRef](#)]
22. Fardhyanti, D.S.; Putri, R.D.A.; Fianti, O.; Simalango, A.F.; Akhir, A.E. Synthesis of silica powder from sugar cane bagasseash and its application as adsorbent in adsorptive-distillation of ethanol-water solution. *MATEC Web Conf.* **2018**, *237*, 02002.
23. Costa, J.A.S.; Paranhos, C.M. Systematic evaluation of amorphous silica production from rice husk ashes. *J. Clean. Prod.* **2018**, *192*, 688–697. [[CrossRef](#)]
24. Chandrasekhar, S.A.T.H.Y.; Satyanarayana, K.G.; Pramada, P.N.; Raghavan, P.; Gupta, T.N. Review processing, properties and applications of reactive silica from rice husk—An overview. *J. Mater. Sci.* **2003**, *38*, 3159–3168. [[CrossRef](#)]
25. Athinarayanan, J.; Periasamy, V.S.; Alhazmi, M.; Alatiyah, K.A.; Alshatwi, A.A. Synthesis of biogenic silica nanoparticles from rice husks for biomedical applications. *Ceram. Int.* **2015**, *41*, 275–281. [[CrossRef](#)]

26. Liu, Y.; Guo, Y.; Zhu, Y.; An, D.; Gao, W.; Wang, Z.; Ma, Y.; Wang, Z. A sustainable route for the preparation of activated carbon and silica from rice husk ash. *J. Hazard. Mater.* **2011**, *186*, 1314–1319. [[CrossRef](#)]
27. Lu, P.; Hsieh, Y.L. Highly pure amorphous silica nano-disks from rice straw. *Powder Technol.* **2012**, *225*, 149–155. [[CrossRef](#)]
28. Kaya, G.G.; Yilmaz, E.; Deveci, H. Sustainable nanocomposites of epoxy and silica xerogel synthesized from corn stalk ash: Enhanced thermal and acoustic insulation performance. *Compos. Part B Eng.* **2018**, *150*, 1–6. [[CrossRef](#)]
29. Salakhum, S.; Yuthalekha, T.; Chareonpanich, M.; Limtrakul, J.; Wattanakit, C. Synthesis of hierarchical faujasite nanosheets from corn cob ash-derived nanosilica as efficient catalysts for hydrogenation of lignin-derived alkylphenols. *Microporous Mesoporous Mater.* **2018**, *258*, 141–150. [[CrossRef](#)]
30. Velmurugan, P.; Shim, J.; Lee, K.J.; Cho, M.; Lim, S.S.; Seo, S.K.; Cho, K.M.; Bang, K.S.; Oh, B.T. Extraction, characterization, and catalytic potential of amorphous silica from corn cobs by sol–gel method. *J. Ind. Eng. Chem.* **2015**, *29*, 298–303. [[CrossRef](#)]
31. Okoronkwo, E.A.; Imoisili, P.E.; Olusunle, S.O.O. Extraction and characterization of amorphous silica from corn cob ash by sol–gel method. *Chem. Mater. Res.* **2013**, *3*, 68–72.
32. Okoronkwo, E.A.; Imoisili, P.E.; Olubayode, S.A.; Olusunle, S.O.O. Development of silica nanoparticle from corn cob ash. *Adv. Nanopart.* **2016**, *5*, 135–139. [[CrossRef](#)]
33. Affandi, S.; Setyawan, H.; Winardi, S.; Purwanto, A.; Balgis, R. A facile method for production of high-purity silica xerogels from bagasse ash. *Adv. Powder Technol.* **2009**, *20*, 468–472. [[CrossRef](#)]
34. Zulfikar, U.; Subhani, T.; Husain, S.W. Synthesis and characterization of silica nanoparticles from clay. *J. Asian Ceram. Soc.* **2016**, *4*, 91–96. [[CrossRef](#)]
35. Kaliannan, D.; Palaninaicker, S.; Palanivel, V.; Mahadeo, M.A.; Ravindra, B.N.; Jae-Jin, S. A novel approach to preparation of nano-adsorbent from agricultural wastes (*Saccharum officinarum* leaves) and its environmental application. *Environ. Sci. Pollut. Res.* **2018**, *26*, 5305–5314. [[CrossRef](#)]
36. Terzioğlu, P.; Yücel, S.; Kuş, Ç. Review on a novel biosilica source for production of advanced silica-based materials: Wheat husk. *Asia-Pac. J. Chem. Eng.* **2018**, *14*, e2262. [[CrossRef](#)]
37. Marag, R.K.; Giri, P.A. Experimental investigation of temperature and reaction time for preparation of silica from wheat husk. *Int. J. Eng. Technol. Sci. Res.* **2018**, *5*, 60–65.
38. Qi, G.; Lei, X.; Li, L.; Sun, Y.; Yuan, C.; Wang, B.; Yin, L.; Xu, H.; Wang, Y. Coal fly ash-derived mesoporous calcium-silicate material (MCSM) for the efficient removal of Cd (II), Cr (III), Ni (II) and Pb (II) from acidic solutions. *Procedia Environ. Sci.* **2016**, *31*, 567–576. [[CrossRef](#)]
39. Li, G.; Wang, B.; Sun, Q.; Xu, W.; Han, Y. Adsorption of lead ion on amino-functionalized fly-440 ash-based SBA-15 mesoporous molecular sieves prepared via two-step hydrothermal method. *Microporous Mesoporous Mater.* **2017**, *252*, 105–115. [[CrossRef](#)]
40. Wang, B.; Zhou, Y.; Li, L.; Xu, H.; Sun, Y.; Wang, Y. Novel synthesis of cyano-functionalized 443 mesoporous silica nanospheres (MSN) from coal fly ash for removal of toxic metals from wastewater. *J. Hazard. Mater.* **2018**, *345*, 76–86. [[CrossRef](#)]
41. Asl, S.M.H.; Javadian, H.; Khavarpour, M.; Belviso, C.; Taghavi, M.; Maghsudi, M. Porous 446 adsorbents derived from coal fly ash as cost-effective and environmentally-friendly sources of aluminosilicate for sequestration of aqueous and gaseous pollutants: A review. *J. Clean. Prod.* **2019**, *208*, 1131–1147. [[CrossRef](#)]
42. Majchrzak-Kuceba, I.; Nowak, W. Characterization of MCM-41 mesoporous materials derived from polish fly ashes. *Int. J. Miner. Process.* **2011**, *101*, 100–111. [[CrossRef](#)]
43. Hua, M.; Zhang, S.; Pan, B.; Zhang, W.; Lv, L.; Zhang, Q. Heavy metal removal from water/wastewater by nano-sized metal oxides: A review. *J. Hazard. Mater.* **2012**, *211*, 317–331. [[CrossRef](#)]
44. Fu, F.; Wang, Q. Removal of heavy metal ions from wastewaters: A review. *J. Environ. Manag.* **2011**, *92*, 407–418. [[CrossRef](#)]
45. Immamuglu, M.; Tekir, O. Removal of copper (II) and lead (II) ions from aqueous solutions by adsorption on activated carbon from a new precursor hazelnut husks. *Desalination* **2008**, *228*, 108–113. [[CrossRef](#)]
46. Kadirvelu, K.; Goe, J.; Rajagopal, C. Sorption of lead, mercury and cadmium ions in multi-component system using carbon aerogel as adsorbent. *J. Hazard. Mater.* **2008**, *153*, 502–507. [[CrossRef](#)]
47. Chingombe, P.; Saha, B.; Wakeman, R. Surface modification and characterization of a coal-based activated carbon. *Carbon* **2005**, *43*, 3132–3143. [[CrossRef](#)]
48. Walker, A.; Wheelock, T.D. Separation of Carbon from Fly Ash Using Froth Flotation. *Coal Prep.* **2006**, *26*, 235–250. [[CrossRef](#)]
49. Huffman, G.P.; Huggins, F.E.; Dunmyre, G.R. Investigation of the high-temperature behavior of coal fly ash in reducing and oxidizing atmospheres. *Fuel* **1991**, *60*, 585–597. [[CrossRef](#)]
50. Catauro, M.; Tranquillo, E.; Risoluti, R.; Vecchio Cipriotti, S. Sol-Gel Synthesis, Spectroscopic and Thermal Behavior Study of SiO₂/PEG Composites Containing Different Amount of Chlorogenic Acid. *Polymers* **2018**, *10*, 682. [[CrossRef](#)]
51. Catauro, M.; D'Angelo, A.; Fiorentino, M.; Gullifa, G.; Risoluti, R.; Vecchio Cipriotti, S. Thermal behavior, morphology and antibacterial properties study of silica/ quercetin nanocomposite materials prepared by sol–gel route. *J. Therm. Anal. Calorim.* **2022**, *147*, 5337–5350. [[CrossRef](#)]
52. Zhu, G.R.; Tan, W.; Sun, J.M.; Gong, Y.B.; Zhang, S.; Zhang, Z.J.; Liu, L.Y. Effects and mechanism research of the desilication pre-treatment for high-aluminum fly ash. *Energy Fuel* **2013**, *27*, 6948–6954. [[CrossRef](#)]
53. Gutzov, S.; Danchova, N.; Karakashev, S.; Khristov, M.; Ivanova, J.; Ulbikas, J. Preparation and thermal properties of chemically prepared nanoporous silica aerogels. *J. Sol-Gel Sci. Technol.* **2014**, *70*, 511–516. [[CrossRef](#)]
54. Maj, S. Energy gap and density in SiO₂ polymorphs. *Phys. Chem. Miner.* **1988**, *15*, 271–273. [[CrossRef](#)]

55. Khedkar, M.V.; Somvanshi, S.B.; Humbe, A.V.; Jadhav, K.M. Surface Modified Sodium Silicate Based Superhydrophobic Silica Aerogels Prepared via Ambient Pressure Drying Process. *J. Non-Cryst. Solids* **2019**, *511*, 140–146. [[CrossRef](#)]
56. Sharafudeen, R.; Al-Hashim, J.M.; Al-Harbi, M.O.; Al-Ajwad, A.I.; Al-Waheed, A.A. Preparation and characterization of precipitated silica using sodium silicate prepared from Saudi Arabian desert sand. *Silicon* **2017**, *9*, 917–922. [[CrossRef](#)]
57. Yan, Z.; Fu, L.; Yang, H.; Ouyang, J. Amino-functionalized hierarchical porous SiO₂-AlOOH composite nanosheets with enhanced adsorption performance. *J. Hazard. Mater.* **2018**, *344*, 1090–1100. [[CrossRef](#)]
58. Tang, H.; Chang, S.; Wu, K.; Tang, G.; Fu, Y.; Liu, Q.; Yang, X. Band gap and morphology engineering of TiO₂ by silica and fluorine co-doping for efficient ultraviolet and visible photocatalysis. *RSC Adv.* **2016**, *6*, 63117–63130. [[CrossRef](#)]
59. Imoisili, P.E.; Ukoba, K.O.; Jen, T.C. Green technology extraction and characterisation of silica nanoparticles from palm kernel shell ash via sol–gel. *J. Mater. Res. Technol.* **2020**, *9*, 307–313. [[CrossRef](#)]
60. Zhang, H.; Zhao, X.; Ding, X.; Lei, H.; Chen, X.; An, D.; Li, Y.; Wang, Z. Preparation and characterization of nano-structured silica from rice husk. *Bioresour. Technol.* **2010**, *101*, 1263–1267. [[CrossRef](#)]
61. Mourhly, A.; Jhilal, F.; El Hamidi, A.; Halim, M.; Arsalane, S. Highly efficient production of mesoporous nano-silica from unconventional resource: Process optimization using a central composite design. *Microchem. J.* **2019**, *145*, 139–145. [[CrossRef](#)]
62. Imoisili, P.E.; Jen, T.-C. Microwave-assisted sol–gel template-free synthesis and characterization of silica nanoparticles obtained from South African coal fly ash. *Nanotechnol. Rev.* **2022**, *11*, 3042–3052. [[CrossRef](#)]
63. Gao, G.M.; Zou, H.F.; Gan, S.C.; Liu, Z.J.; An, B.C.; Xu, J.J.; Li, G.H. Preparation and properties of silica nanoparticles from oil shale ash. *Powder Technol.* **2009**, *191*, 47–51. [[CrossRef](#)]